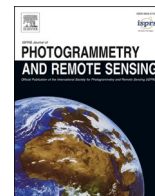


Contents lists available at [ScienceDirect](https://www.sciencedirect.com)

ISPRS Journal of Photogrammetry and Remote Sensing

journal homepage: www.elsevier.com/locate/isprsjprs

Towards spatially continuous mapping of soil organic carbon in croplands using multitemporal Sentinel-2 remote sensing

Pu Shi^{a,*}, Johan Six^b, Andrew Sila^c, Bernard Vanlauwe^d, Kristof Van Oost^a^a Georges Lemaître Centre for Earth and Climate Research, Earth and Life Institute, Université catholique de Louvain, 1348 Louvain-la-Neuve, Belgium^b Department of Environmental Systems Science, ETH Zurich, 8092 Zurich, Switzerland^c World Agroforestry Centre (ICRAF), PO Box 30677, Nairobi 00100, Kenya^d International Institute of Tropical Agriculture (IITA), PO Box 30772, Nairobi 00100, Kenya

ARTICLE INFO

Keywords:

Sentinel-2

Soil organic carbon mapping

Multitemporal analysis

Bare soil composite

ABSTRACT

Intensified human activities can augment soil organic carbon (SOC) losses from the world's croplands, making SOC a highly dynamic parameter both in space and time. Sentinel-2 spectral imagery is well placed to capture the spatiotemporal variability of SOC, but its capability has only been demonstrated for agricultural regions mostly located in Europe. Furthermore, most studies so far only used single-date images that resulted in spatially non-continuous SOC maps, hampering their ability to aid multiscale SOC assessments. Here, we aim to achieve spatially continuous mapping of SOC in croplands, by creating multitemporal bare soil composites that maximize cropland coverage in two regions of varying agroecosystems and landscape structure in the Northeast China Chernozem region and the Belgian Loam Belt. Bare soil pixels were extracted via spectral index thresholding that excluded contaminated pixels from external perturbation. Multitemporal soil composites were then obtained by averaging over multiple single-date bare soil images that were selected within pre-determined optimal time-windows, corresponding to the region-specific crop sowing periods when best possible surface conditions were expected. Results show that the optimal time-window filter ensured selective inclusion of single-date images that themselves yielded stable and robust SOC predictions across multiple years. Spectral-based models developed from multitemporal composites consistently produced better or similar prediction accuracies than single-date images for both study regions (R^2 : 0.52–0.62; RMSE: 0.17–0.21 g 100 g⁻¹), while also achieved maximum cropland coverage (>82 %). Bootstrap modelling demonstrated that SOC mapping via multitemporal Sentinel-2 data was associated with small uncertainties. Investigations into the significant spectral bands that contributed to the prediction of SOC suggested that, regardless of the study regions, the physical relationship between spectral bands and SOC that predominantly exists for laboratory spectra is largely translated into Sentinel-2 platforms. This study highlights the widespread applicability of multitemporal Sentinel-2 remote sensing for effective and high-resolution SOC mapping, in order to detect localized soil degradation as well as to inform regional cropland management in diverse agroecosystems.

1. Introduction

Intensified human activities can augment the vertical soil-atmosphere carbon flux as well as the lateral redistribution of soil organic carbon (SOC) by earth surface processes (Van Oost et al., 2007; Yue et al., 2016), making SOC a highly dynamic parameter both in space and time. This is particularly relevant for the world's croplands, where the ever-increasing human pressure exerts significant disturbances to SOC dynamics, threatening food security and its functions to provide ecosystem services and mitigate climate change (Lal, 2004; Lorenz et al.,

2019). Thus, there is an increasing demand to quantify SOC at high spatial resolution in order to detect localized soil degradation and monitor the temporal change in SOC at scales relevant for sustainable cropland management.

Laboratory visible, near-, and short-wave infrared (VNIR/SWIR) spectroscopy has become a widely adopted approach to rapidly and accurately determine primary soil properties, especially SOC (Soriano-Disla et al., 2014). Evaluations on whether the success established in the laboratory could be translated into remote sensing platforms have shown that the spatial variability of SOC from field to landscape scales

* Corresponding author.

E-mail address: pu.shi@uclouvain.be (P. Shi).<https://doi.org/10.1016/j.isprsjprs.2022.09.013>

Received 6 May 2022; Received in revised form 22 July 2022; Accepted 16 September 2022

Available online 26 September 2022

0924-2716/© 2022 International Society for Photogrammetry and Remote Sensing, Inc. (ISPRS). Published by Elsevier B.V. All rights reserved.

could be reliably captured with both air- and spaceborne spectral imagery (Angelopoulos et al., 2019). Compared to the conventional digital soil mapping methods that are often constrained by dated and/or inconsistent soil data (Arrouays et al., 2014; Vågen et al., 2016), soil mapping based on spectral imaging relies on the physical link between soil spectral reflectance in the VNIR/SWIR region and soil chromophores at pixel level (Ben-Dor et al., 2009; Chabrilat et al., 2019); thus providing robust, up-to-date and spatially explicit information needed for SOC monitoring and assessment.

The launch of the Sentinel-2 super spectral satellite in 2015 has opened a new arena of opportunities for large-scale, high-resolution soil mapping, as it provides continuous data streams of global surface reflectance at improved spatial, spectral and temporal resolution in comparison to its counterparts such as Landsat 8 (Helder et al., 2018). The Sentinel-2 spectral bands span across the VNIR/SWIR region, including two SWIR bands at around 1600 and 2200 nm, which are known to be highly sensitive to SOC variation (Ben-Dor et al., 1997). Pilot studies have demonstrated the potential of Sentinel-2 imagery to reproduce the spatial pattern of SOC both at field scale and across wider landscapes (Castaldi et al., 2019b; Vaudour et al., 2019a), particularly for regions with high and variable SOC values (Gholizadeh et al., 2018). Recent work also developed bottom-up approaches to link existing soil spectral libraries with Sentinel-2 spectra (Castaldi et al., 2019a; Tziolas et al., 2020). However, most of these studies were carried out in high-input agricultural systems across Europe, little research has been conducted on how and to what extent Sentinel-2 imagery can facilitate high-resolution SOC mapping in other continents, where interferences may arise from a large heterogeneity in soil surface conditions and landscape structure.

Another research gap in using Sentinel-2 imagery for SOC mapping lies in the fact that most studies so far only used single-date images for this task. The major issue associated with the use of single-date images is the limited availability of bare soil pixels at a given time (Tziolas et al., 2020; Vaudour et al., 2019a) due to varying crop rotations between neighboring fields. The direct product resulting from one single-date image is thus a spatially non-continuous SOC map, hampering its potential to aid in better targeting cropland management. In this context, Diek et al. (2016) combined three airborne hyperspectral image acquisitions to create a multitemporal bare soil composite that doubled the bare soil coverage as compared to single-date images. Upscaling to national scale, Rogge et al. (2018) used Landsat legacy data to build bare soil composites of Germany at 5-year intervals for monitoring the temporal evolution of cropland extent within 30 years. They created minimum and maximum modified Normalized Difference Vegetation Index (NDVI) composites, which were later intersected to separate bare cropland from other land use classes such as built-up areas (including urban areas, rural villages, and road networks) and forests. With a similar objective, Dematté et al. (2018) designed the GEOS3 processor to create a multitemporal bare soil mosaic with 68 % cropland coverage of the study area. Such bare pixel compositing methodologies have since been applied in various contexts for topsoil mapping, but primarily with Landsat products (Rizzo et al., 2020; Safanelli et al., 2020). Silvero et al. (2021) recently attempted to combine Sentinel-2 with Landsat 8 to obtain a soil reflectance composite that improved soil prediction models with two times larger bare soil area covered than those obtained from single-date images. Moreover, Vaudour et al. (2021) tested several image temporal-mosaicking strategies, including the utilization of Sentinel-1 data to account for soil moisture variation, to maximize cropland coverage while maintaining good SOC prediction accuracy.

The remaining challenge with creating above-mentioned bare soil composites for soil mapping purposes arises from the temporal inconsistencies in spectral characteristics caused by disturbing factors such as crop residue, soil moisture and surface roughness (Chabrilat et al., 2019; Diek et al., 2019; Vaudour et al., 2019b). Ignoring the effects of such perturbing factors as crop residue on the purity of soil spectra could lead to systematic overestimation of SOC (Dvorakova

et al., 2020). Vaudour et al. (2019b) assessed the impact of Sentinel-2 image acquisition date on the predictive performance of SOC in the Versailles Plain, France, and found that images acquired within a period of several months produced drastically different results and the best model performance was obtained in March-April, coinciding with the crop sowing period with optimal soil surface condition. Gomez et al. (2019) also tested Sentinel-2 images from varying months and found that considerable uncertainties were associated with soil texture prediction, due to changing soil surface conditions over time that interfered with the “true” soil spectra. To account for this problem, Dematté et al. (2018) used the Normalized Burn Ratio 2 (NBR2) index, also known as the normalized difference tillage index (NDTI) (Van Deventer et al., 1997), to remove soil pixels that are “contaminated” by crop residue and soil moisture. Castaldi et al. (2019a) found that stricter NBR2 thresholding led to better SOC prediction, but a smaller number of available calibration samples and thus limited coverage of bare soil area by single-date Sentinel-2 images.

Hence, the road to accurate and spatially continuous SOC mapping using Sentinel-2 imagery requires (i) selecting images within the optimal time window when the largest percentage of bare soils is exposed, ideally at seedbed condition before crop sowing; (ii) using spectral index (e.g. NDVI and NBR2) thresholding to further refine bare soil pixels by removing the spectral noise from perturbing factors; and finally (iii) mosaicking the refined single-date images to create a multitemporal bare soil composite with maximized cropland area. Previous studies have addressed these requirements separately but rarely all at once to achieve a consolidated framework, particularly in agroecosystems of different continents, where the general applicability of such a framework is confronted with additional constraint posed by the varying soil surface management and landscape structure. For instance, as opposed to previous applications demonstrated in European croplands characterized by elevated fertilization and intensive management, to what extent would Sentinel-2 based SOC predictive modelling be able to capture the spatial variability of SOC in largely degraded croplands?

In this study, we aim to address these requirements simultaneously in an attempt towards spatially continuous mapping of SOC in croplands of different agroecosystems. To this end, a methodological framework, including delineation of cropland extent, detection of bare soil pixels with minimal disturbance and creation of multitemporal bare soil composite for SOC mapping was first developed for the Chernozem region of Northeast (NE) China, one of the most seriously degraded agricultural regions in the country. The transferability of such an approach was then tested in a typical European agricultural area located in the Belgian Loam Belt. Particular focus was given to (i) testing the consistency of Sentinel-2 data when selected within the optimal time window over three successive years; and (ii) the assessment of the accuracy and uncertainty of SOC prediction between composited and single-date soil spectra.

2. Study regions

The two selected study regions, one in NE China and the other in Belgian Loam Belt, are both characterized by loess-derived loamy soils and rolling topography, both under prolonged intensive cultivation, and in need for spatially resolved SOC monitoring and assessment platform to aid sustainable agricultural management. They differ, however, in two key aspects: (1) croplands in NE China are mostly sown once a year with long periods of bare soil exposure in spring, while Belgium Loam Belt is characterized by a more diverse cropping system; (2) in comparison to the Belgian study region dominated by Luvisols with relatively lower average SOC content, soils in NE China are characterized by fertile Chernozems and Phaeozems but under higher degree of soil erosion due to improper management (Borrelli et al., 2020). As a result, soils in this region are among the most severely degraded in the country. Erosion-induced soil redistribution have caused significant decline in and a spatial re-organization of SOC (Ou et al., 2017), making this region

an ideal location, and a contrast to the Belgian Loam Belt, to assess the capability of Sentinel-2 remote sensing in driving the new generation of SOC mapping. More specific site characteristics of the two study regions are given below.

2.1. Chernozem region in Northeast China

The study area (ca. 10 000 km², 44.22 N-44.83 N, 124.76E-126.33E) located in the Chernozem region of NE China (Fig. 1a) is an important grain base in the country, with maize being the dominant crop. The climate is temperate continental monsoon with mean temperatures ranging from -11 °C in January to 25 °C in July, and the mean annual precipitation is 577 mm. The crop calendar for maize spans from April to October, and vast areas of bare croplands are exposed in April-May as farmers prepare the seedbed for maize sowing.

2.2. Belgian Loam Belt

The Belgian study area is located in the Loam Belt in the central part of Belgium (Fig. 1b). It occupies a rectangular area of ca. 230 km² (SW corner: 50.60 N, 4.65E; NE corner:50.70 N, 5.06E) that is characterized by a temperate oceanic climate with a mean annual precipitation of 790 mm, and mean temperatures between 2.3 °C (January) and 17.8 °C (July). Large areas of bare croplands are usually found in two time-windows of each year, the first in May before the sowing of maize and the second in late August to September before the planting of winter wheat and winter barley.

2.3. Soil sampling and analyses

To establish the ground-reference datasets needed for the development of Sentinel-2 based SOC prediction models, soil sampling campaigns were carried out in May 2019 in NE China and in October 2018 and 2019 in the Belgian Loam Belt. Spatial distribution of the soil sampling points is given in Fig. 1, and the number of samples in Table 1. For both study regions, a stratified random sampling design was adopted to cover different levels of SOC concentration according to SOC data from the SoilGrids250m product (Hengl et al., 2017). Each bulk sample, consisting of five sub-samples taken in a 2 m radius, was taken at 0–10 cm depth, then air-dried and passed through a 2 mm sieve. Total C concentration of ground soil samples (<100 μm) was measured with a VarioMax CN analyzer (Elementar GmbH, Langensfeld, Germany). For the samples that showed clear reactions under 10 % HCl treatment,

inorganic C content was determined using a modified pressure-calcimeter method (Sherrod et al., 2002). SOC was then obtained by the subtraction of inorganic C from total C. Laboratory VNIR/SWIR spectra were also acquired on the sieved (<2 mm) samples for the two regions, using an ASD Fieldspec 3 FR spectroradiometer (Analytical Spectral Devices Inc., USA). Details on the instrument set-up and measurement procedure are given in Shi et al. (2020b).

3. Methodology

Fig. 2 depicts the general workflow of the methodology. Three interconnected main steps, consisting of image pre-processing, cropland extent extraction and creation of bare soil composite, are structured in a way that the product from the preceding step was fed into the next. Details on the approach are in the following.

3.1. Sentinel-2 image pre-processing

Sentinel-2 Multi-Spectral Imager constellation currently comprises two satellites (2A and 2B) providing data with 13 VNIR/SWIR bands at approximately-five-day revisit time. For the two study regions, Level-1C products within the period from January 1, 2018 to May 15, 2020 were downloaded, and atmospherically corrected to Level-2A products, i.e. Bottom-of-Atmosphere reflectance, using the Sen2Cor processor (standalone version 2.8). A cloud filter of <10 % was applied to exclude images with excessive cloud coverage, and the Scene Classification Layer output from the Sen2Cor algorithm was used to further remove pixels that were recognized as clouds, cloud shadow, dark feature shadow and thin cirrus. As a result, 27 cloud-free scenes were obtained in NE China, while 22 scenes were available for the Belgian Loam Belt (Table 1). Finally, 10 bands covering the visible (B2, B3, B4), red-edge (B5, B6, B7), NIR (B8, B8A) and SWIR (B11, B12) regions were selected as explanatory variables for SOC prediction. All the bands were spatially resampled at 10 m by nearest neighbor using the SNAP software.

3.2. Delineation of cropland extent

To create the cropland spatial extent, other land use classes needed to be detected and excluded, usually by setting critical spectral index thresholds. While NDVI has been widely used to distinguish bare soils from photosynthetic vegetation (Shi et al., 2020a), built-up area has significant overlap with bare soil in low NDVI values. To tackle this

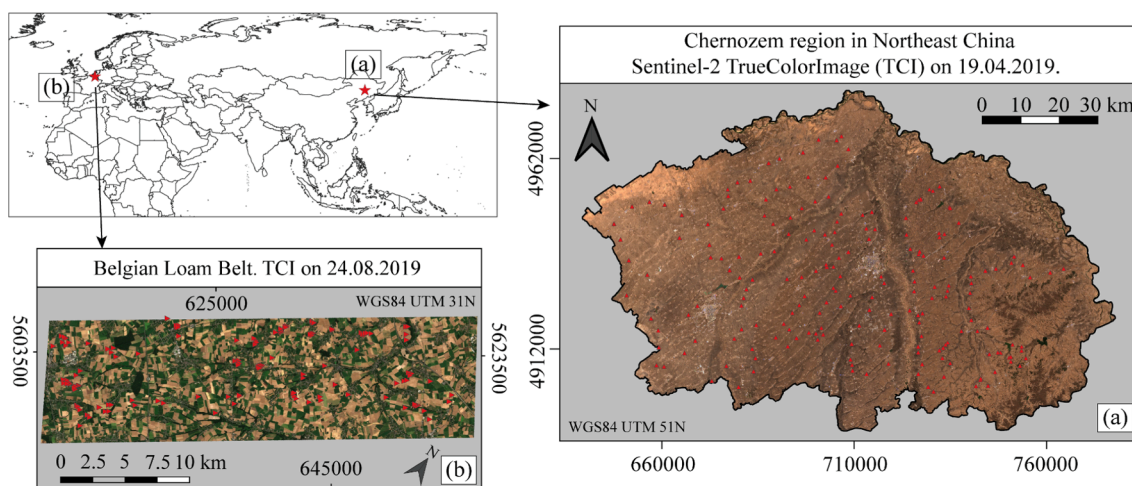


Fig. 1. Geographic location of the two study regions in (a) the Chernozem region of Northeast China and (b) the Belgian Loam Belt. The spatial distribution of soil sampling points (red triangles) within each study region was overlaid onto the respective Sentinel-2 true color image of a specific date. (For interpretation of the references to color in this figure legend, the reader is referred to the web version of this article.)

Table 1

Summary statistics of soil organic carbon content and number of samples and Sentinel-2 scenes used in this study. Q1 and Q3 denote the 1st and 3rd quantile. SD: standard deviation.

| Study region | Sample size | Soil organic carbon (g/100 g) | | | | | | | | N° of Sentinel-2 scenes |
|-------------------|-------------|-------------------------------|------|------|--------|------|------|------|----------|-------------------------|
| | | Min | Q1 | Mean | Median | Q3 | Max | SD | Skewness | |
| Northeast China | 203 | 0.64 | 1.32 | 1.51 | 1.50 | 1.69 | 2.51 | 0.28 | 0.23 | 27 |
| Belgian Loam Belt | 137 | 0.67 | 0.99 | 1.36 | 1.18 | 1.51 | 2.55 | 0.67 | 1.16 | 22 |

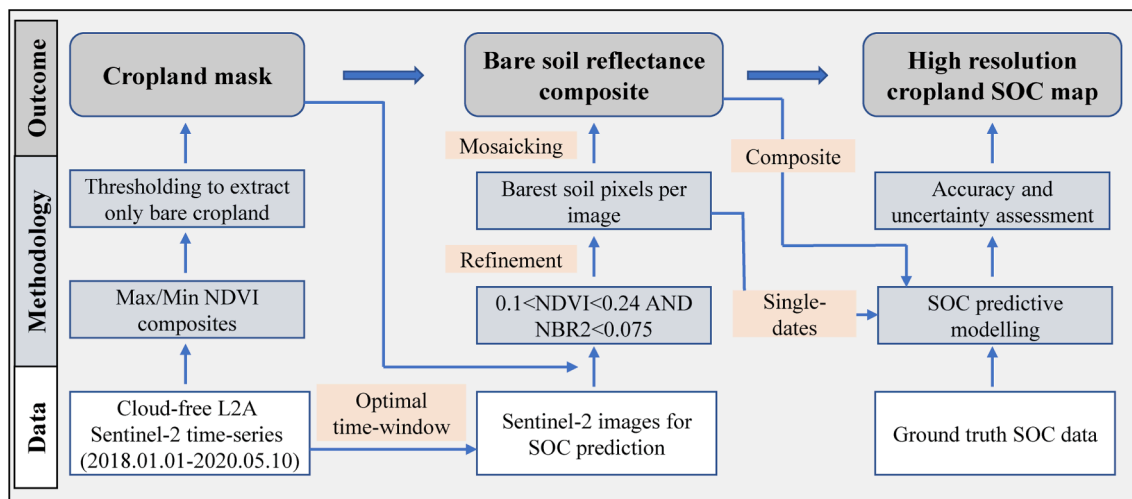


Fig. 2. Flowchart of the three main steps (as indicated by the thick blue arrow) to produce a spatially continuous soil organic carbon (SOC) map. NDVI: Normalized Difference Vegetation Index; NBR2: Normalized Burn Ratio 2. (For interpretation of the references to color in this figure legend, the reader is referred to the web version of this article.)

problem, we followed the principal outlined by Rogge et al. (2018), who took advantage of the distinct pattern of NDVI time-series for different land use classes. Specifically, maximum and minimum NDVI composites (NDVImax and NDVimin) were created from NDVI time-series, and pixels that have high values in the NDVImax composite and low values in the NDVimin composite were intersected to create a mask that is only composed of bare cropland soil pixels. This method is particularly useful for areas where up-to-date information on land cover is scarce. Details on the implementation of the method can be found in Rogge et al. (2018).

To verify the method, the processed Sentinel-2 images for NE China were used to establish a NDVI time-series, which were later used to create the NDVImax and NDVimin composites. NDVI characteristics of cropland, forests, and built-up area were investigated to determine the critical threshold for bare soil. 2000 points per land use class were randomly selected based on the 2019 Land Use Distribution vector map provided by the Department of Natural Resources, Jilin Province. NDVI values for those selected points were extracted from the NDVI composites as plotted in Fig. 3. For the NDVimin composite, it can be seen that NDVI values representative of bare croplands fell in the range of 0.10–0.24, which can be used to clearly differentiate bare cropland from forest. Built-up areas generally displayed low NDVI values that did not vary much from NDVimin to NDVImax, as compared to croplands and forests. In this line, a NDVI threshold of <0.75 can thus be determined from NDVImax to exclude the built-up areas and then combined with the NDVI of 0.10–0.24 from NDVimin to delineate the cropland extent. Zoom-in shots on two restricted areas in NE China (Fig. 4a, b) show that the NDVI thresholding resulted in a cropland mask that accurately excluded built-up and forest areas. The same NDVimin and NDVImax thresholds were also applied against the Belgian site and showed good discrimination of croplands from other land use classes (Fig. 4c, d).

3.3. Creation of bare soil composite

The cropland extent created above is used only as a “canvas”, upon which pure bare soil pixels from multiple single-date images were filled to create a multitemporal mosaic of “true” soil spectral reflectance. A two-step refinement procedure was applied to extract the bare soil pixels: (1) only images within the determined optimal time-windows were included for the bare soil pixel compositing; (2) a combination of NDVI and NBR2 thresholds was applied to extract bare soil pixels of the highest possible purity, that is of minimal disturbance from green vegetation, crop residue and soil moisture.

For the first refinement procedure, we define the “optimal time-window” as the period when the largest percentage of bare soils at its optimal surface condition can be found. For this purpose, we extracted the beginning periods of major crop sowing in the study regions based on the FAO crop calendar per country and assumed that soils were at their barest condition when seedbeds were prepared for sowing. The optimal time-window was found in April–May for NE China, and April–May plus September–October for Belgium. Then, the determined time-windows were used as filter to extract the single-date images for SOC modelling. A total of three and four images were extracted for NE China and Belgium from a pool of 27 and 22 images respectively.

For the second refinement procedure, the 0.10–0.24 NDVI range, as identified in Fig. 3, was used to remove green vegetation pixels. This agrees with the study by Shi et al. (2020a), who set a similar NDVI threshold (0.10–0.25) based on investigations on 100 bare fields in the Belgian Loam Belt. Furthermore, temporal evolution of NDVI during the year 2019 was plotted using the same 2000 sampling points as in Fig. 3 for the croplands in NE China. Although similar NDVI occurred in April and October, contrasting distributions of NBR2 values were found in the two time periods (Fig. 5). Higher NBR2 in October was due to the excessive maize stalk residues left on the field after harvest. This suggests that NDVI alone is not sufficient to extract bare soil pixels, and the

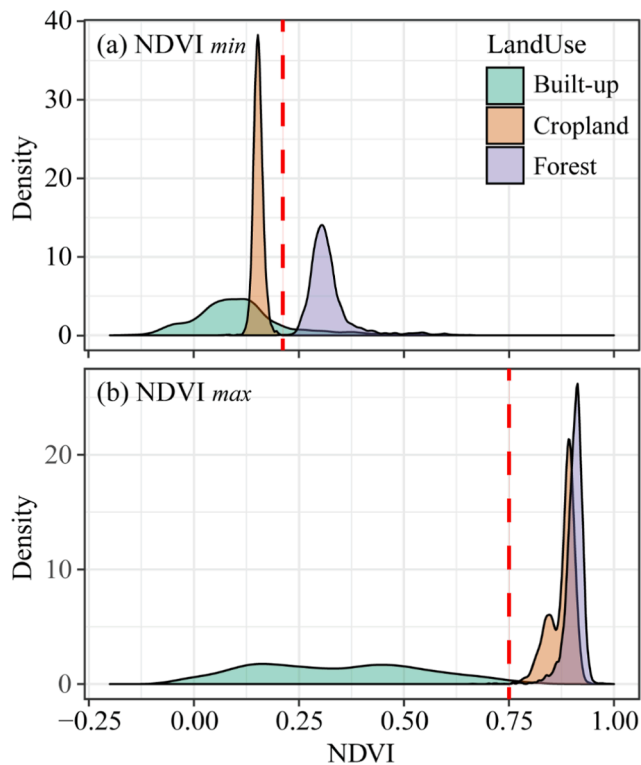


Fig. 3. Density distribution of the normalized difference vegetation index (NDVI) for built-up, cropland, and forest areas in the Northeast China study region. $NDVI_{min}$ (a) and $NDVI_{max}$ (b) denote the minimum and maximum NDVI composites created using the Sentinel-2 time-series (January 2018–May 2020). Density plots were created based on the NDVI characteristics of 2000 randomly sampled points for each land use class based on the 2019 Land Use Distribution vector map in the study area.

NBR2 threshold of 0.075 was adopted to further remove the soil pixels that were “contaminated” by crop residue (Fig. 5b). The same NBR2 threshold was also used by Dematté et al. (2018) to remove noisy pixels in tropical Brazil, and by Castaldi et al. (2019a) who reported that the NBR2 index at 0.075 was the most suitable threshold to produce a good SOC prediction model while concurrently maintaining a relatively high proportion of bare soil coverage in Northern Germany. The consistent adoption of the NBR2 threshold at 0.075 across diverse agroecosystems proved its potential for widespread applications.

Therefore, a combination of NDVI and NBR2 thresholding was applied to each single-date image within the determined optimal time-window. Then, all the processed single-date images were filled into the cropland extent, and a mean multitemporal bare soil composite was created by averaging over the multiple occurrences of bare soil reflectance for each pixel. It should be noted that the procedures described in Sections 3.2 and 3.3 were first developed and verified in NE China, and then applied in the Belgium Loam Belt to create both the single-date bare soil images as well as the multitemporal bare soil composites.

3.4. SOC predictive modelling

3.4.1. Single-date versus multitemporal composite

Sentinel-2 based SOC prediction models were developed using multitemporal bare soil composites as well as every single-date image within the optimal time-window. The reason of developing SOC models with single-date images was twofold: first, to serve as a reference for comparing the model performance with that from multitemporal composites; and second, to assess the temporal consistency of Sentinel-2 data across multiple years. To this end, geographic coordinates of the available soil samples (Table 1) were used to extract Sentinel-2 spectra from

both the bare soil composites and the selected single-date images. For each study region, spectra-based SOC prediction model was built by means of partial least squares regression (PLSR) with 10-fold cross-validation and applied to all the available bare soil pixels to produce SOC maps in 10 m spatial resolution. Percentage of bare soil coverage (PBC) was calculated by dividing the number of pixels in the predicted SOC maps with that in the cropland extent. Lastly, the SOC model calibrated using the 2019 Sentinel-2 data in NE China was evaluated against the 2018 and 2020 data, with the aim to further test the consistency and interchangeability of Sentinel-2 data acquired in different years.

3.4.2. Model performance assessment

To assess the prediction performance of the PLSR models, bootstrap resampling with replacement was adopted to obtain a slightly different dataset each time for model calibration and cross-validation during 100 repeated simulations. Mean predicted SOC values from simulations were reported and standard deviation of the mean was used to indicate the robustness of the PLSR models. The coefficient of determination (R^2) of measured against predicted values, root mean squared error (RMSE), ratio of performance to deviation (RPD), and ratio of performance to interquartile range (RPIQ) were examined to evaluate the model performances. Variance Importance Projection (VIP) index was calculated to identify the spectral regions (VIP greater than 1) that contributed to the prediction of SOC in the PLSR models (Chong and Jun, 2005). In addition, the prediction uncertainties of the PLSR models developed from the multitemporal composites were assessed following the method outlined in Malone et al. (2017), where the average MSE of model predictions was added to the bootstrap prediction variance at each pixel to obtain the overall prediction variance, accounting for the systematic, random and deterministic errors from modelling. The uncertainty was expressed as 90 % prediction intervals, which were the square root of overall prediction variance multiplied by the Z score at 90 % probability. All the statistical analyses, SOC prediction and mapping were conducted with R software.

3.4.3. Resampled Sentinel-2 versus real Sentinel-2

The laboratory VNIR/SWIR (400–2500 nm) spectra for the two study regions were resampled into the same spectral resolution as the Sentinel-2 bands, and SOC models were established and evaluated following the same procedure as described above. In particular, the VIP index was calculated for the PLSR model using both resampled and real Sentinel-2 data, in order to investigate whether the widely acknowledged physical relationship between certain spectral regions and SOC for laboratory spectra would translate to satellite platforms.

4. Results

4.1. Soil organic carbon content in the study regions

Summary statistics on the measured SOC content in the study regions are shown in Table 1. The study region in NE China, as largely characterized by Chernozem soils, had a mean SOC concentration of $1.51 \text{ g } 100 \text{ g}^{-1}$ and a close median, indicating a normally distributed sample set. While, in comparison, the Belgian Loam Belt region had lower mean SOC concentration ($1.36 \text{ g } 100 \text{ g}^{-1}$), and its median SOC was lower than the mean, showing that the SOC distribution for the Belgian study region was slightly skewed towards low SOC levels (skewness: 1.16).

4.2. Sentinel-2 based SOC predictive modelling and mapping

4.2.1. NE China

Three cloud-free Sentinel-2 images within the optimal time window (April–May) during 2018–2020 were selected for model development and for creating the multitemporal bare soil composite. Individual SOC prediction models built with single-date images showed reasonable

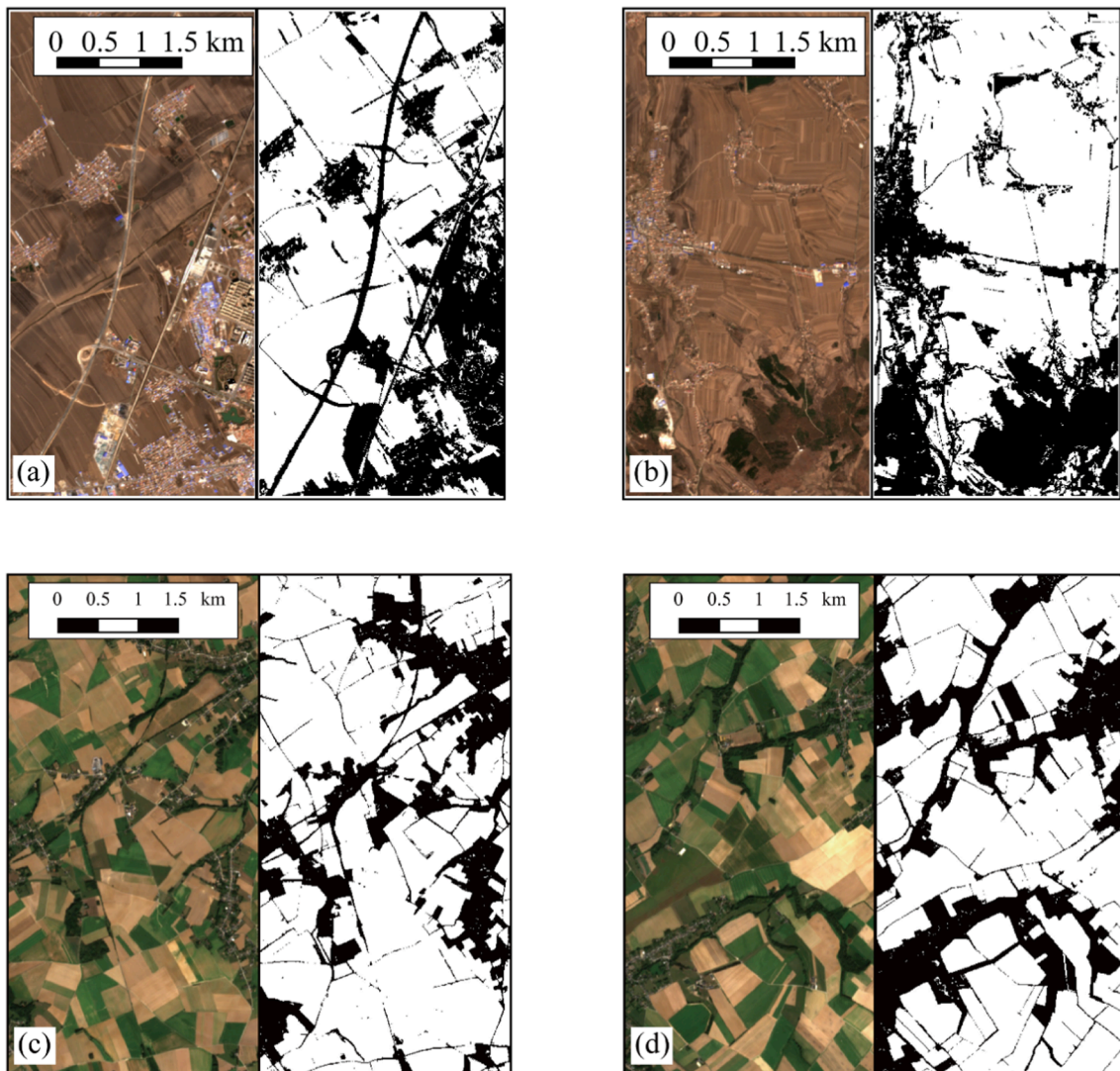


Fig. 4. Zoom-in shots to demonstrate the effectiveness of the delineated cropland mask in (a,b) Northeast China and (c, d) Belgian Loam Belt. The same $NDVI_{min}$ and $NDVI_{max}$ thresholds identified in Fig. 3 were used to delineate the cropland extent for Belgium. Each sub-figure consists of a true color image (left) and a matching binary image (right), depicting the extracted bare cropland extent (white areas) and the excluded forests and built-up areas (black areas).

performances with RMSE smaller than $0.20 \text{ g } 100 \text{ g}^{-1}$, R^2 larger than 0.5, and RPD larger than 1.4 for all three dates (and years) (Table 2). Nearly all of the available soil samples were detected as in bare soil condition, indicating that during the selected time-window, large areas of croplands were prepared for seedbed for crop sowing. This corroborates the validity of determining optimal time-windows, which maximized the number of training samples. As a result, high PBC values ($>80\%$) were consistently observed for the three single-date images in three years in NE China. Moreover, the SOC model calibrated with the 2019 Sentinel-2 image was tested against the 2018 and 2020 images and the validation yielded equally good R^2 but slightly higher RMSE, lower RPD and RPIQ.

The SOC prediction model developed from the multitemporal bare soil composite demonstrated promising capability of Sentinel-2 data for high-resolution SOC mapping. The performance of the PLSR model developed from the multitemporal composite represented broad improvements over the single-date models, as expressed by lower RMSE and higher R^2 , RPD and RPIQ values (Fig. 6). Furthermore, the close match between the regression line and the 1:1 line indicates the unbiasedness of the PLSR model. Finally, the predicted 10 m spatial resolution SOC map is consistent with existing knowledge on the spatial distribution pattern of SOC in this region, with higher SOC values found

close to river valleys.

4.2.2. Belgian Loam Belt

The SOC modelling and mapping procedure used in NE China was applied in the Belgian Loam Belt region, for the purpose of further evaluation on the general applicability of the proposed methodology. According to the cropland calendar of this region, optimal time-windows for maximized bare cropland exposure were found in May and August–September each year during the sown of potatoes, sugar beets, and winter cereals. Similar to the NE China case, all four selected single-date images in the Belgian site gave acceptable results with generally low RMSEs and satisfactory R^2 and RPDs (Fig. 7). But unlike the NE China case, varying numbers of bare soil samples (from 28 to 76) were available to train SOC prediction models, and this led to differing model performances as well. For instance, the largest number of training samples was obtained for the September 2018 image, while the PLSR model from this image also gave the largest RMSE at $0.22 \text{ g } 100 \text{ g}^{-1}$. For the 2019 and 2020 images, more accurate model predictions were obtained with R^2 larger than 0.6 and RMSE as low as $0.14 \text{ g } 100 \text{ g}^{-1}$ in 2020, but this is likely due to the reduction in the size of training samples that led to narrower range of SOC variations, thus not well representing the true population in terms of SOC distribution in the Belgian

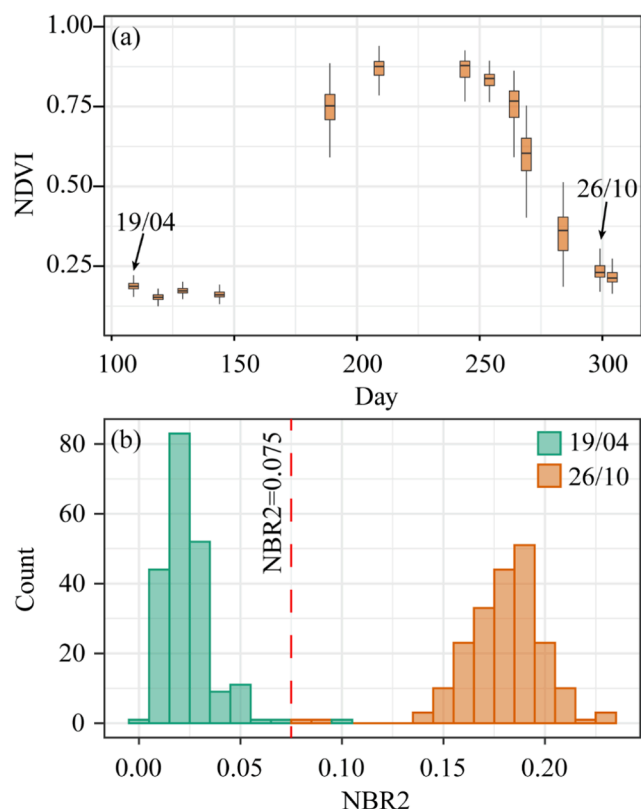


Fig. 5. (a) Temporal evolution of the normalized difference vegetation index (NDVI) for the croplands in the Northeast China study region for the year 2019. The same 2000 cropland points presented in Fig. 3 were used. (b) the normalized burn ratio 2 (NBR2) distribution for the two dates that had similar NDVI range but contrasting NBR2 values.

Table 2

Cross-validation performances of soil organic carbon (SOC) prediction models using single-date Sentinel-2 images in Northeast China. The reported root mean squared error (RMSE), coefficient of determination (R^2) and ratio of performance to interquartile range (RPIQ) values are the mean values \pm the standard deviations resulting from 100 bootstrapped model simulations.

| Image acquisition date | N° of training samples | RMSE (g/100 g) | R^2 | RPD | RPIQ | Percentage of bare soil coverage within the bare cropland extent |
|--|------------------------|-----------------|-----------------|-----------------|-----------------|--|
| 24/04/2018 | 198 | 0.19 \pm 0.01 | 0.53 \pm 0.06 | 1.48 \pm 0.09 | 1.91 \pm 0.18 | 91 % |
| 19/04/2019 | 201 | 0.18 \pm 0.01 | 0.59 \pm 0.04 | 1.57 \pm 0.08 | 2.08 \pm 0.16 | 94 % |
| 13/05/2020 | 197 | 0.19 \pm 0.01 | 0.51 \pm 0.06 | 1.44 \pm 0.09 | 1.90 \pm 0.17 | 81 % |
| Applicability of SOC prediction model built with 2019 Sentinel-2 data to other years | | | | | | |
| 24/04/2018 | 198 | 0.23 | 0.53 | 1.15 | 1.49 | 91 % |
| 13/05/2020 | 197 | 0.23 | 0.52 | 1.19 | 1.57 | 81 % |

region.

When upgrading from single-date to multitemporal composite, the most striking result was the roughly-two-times increase in PBC from 35 % to 45 % among the single-date images to 82 % for the multitemporal

composite. With the substantial improvement in the area of bare soil covered, the model accuracy maintained at the similar level (RMSE: 0.21 g 100 g⁻¹) to that from the single-date images (Fig. 7). The regression line again fit almost perfectly with the 1:1 line, although there seemed to be some underestimation of the high SOC values.

4.3. Comparison of SOC predictions between resampled and real Sentinel-2 data

SOC prediction models were also established using the resampled Sentinel-2 data for the NE China and Belgian regions, and it was found that the PLSR models had similar levels of accuracy as those developed with real Sentinel-2 data, with identical RMSEs at 0.17 and 0.21 g 100 g⁻¹ for NE China and Belgium (Fig. 8). The VIP figure showed a similar pattern for both resampled and real Sentinel-2 data, with NIR and SWIR bands (B8A, B11, B12) being significant predictors in the PLSR models, whereas the red-edge bands (B5-B7) remained non-significant for both study regions. Apart from the similarities, the visible bands from the resampled Sentinel-2 data seemed to have played a relatively more important role in predicting SOC than the visible bands from the real Sentinel-2 data.

4.4. Uncertainty assessment of SOC prediction

The 100 bootstrapped model simulations enabled assessments both on the robustness of the developed PLSR models and their overall prediction uncertainties. As shown in Figs. 6 and 7, the mean predicted SOC values for both study regions were associated with small standard deviations (indicated by the error bars) from bootstrapping, highlighting the robustness of the SOC prediction models based on Sentinel-2 derived spectra, especially for the NE China region. Furthermore, the uncertainty maps (Fig. 9), as expressed by 90 % prediction interval, could allow assessments of SOC modelling from a spatial perspective. A majority of the areas in both regions were characterized by narrow range of prediction intervals (<0.3 g 100⁻¹), but comparatively speaking, the SOC map of NE China on average had lower prediction uncertainty than that of Belgium. Areas with relatively higher uncertainties are commonly found along field boundaries for both regions, but also in the northeast and northwest corners of NE China and individual fields of Belgium with no clear spatial pattern.

5. Discussion

5.1. Capability of multitemporal Sentinel-2 remote sensing for SOC mapping

The selected single-date images within the optimal time-windows for the NE China and Belgian study regions consistently produced satisfactory SOC prediction models with small RMSEs (0.14–0.22 g 100 g⁻¹). Considering the narrow range of variation in SOC for the NE China region and the generally low SOC content for the Belgian region, the fact that a large part of SOC variability was captured by the prediction models highlights the promising potential of Sentinel-2 remote sensing for high spatial resolution SOC mapping. Furthermore, single-date Sentinel-2 images across multiple years yielded comparable SOC prediction accuracies (Table 2) means that a high level of interannual data consistency and stability can be expected when images were properly processed for noise removal and selected within the optimal time-windows. This was further supported by the good model transferability among the multiple single-date images when the PLSR model calibrated using the 2019 data was validated against the 2018 and 2020 data in NE China. This implies that the Sentinel-2 soil reflectance from different years could be used interchangeably if a slight decrease in model accuracy is tolerated.

The consistent good performance achieved from SOC prediction models built with single-date images also justified the creation of

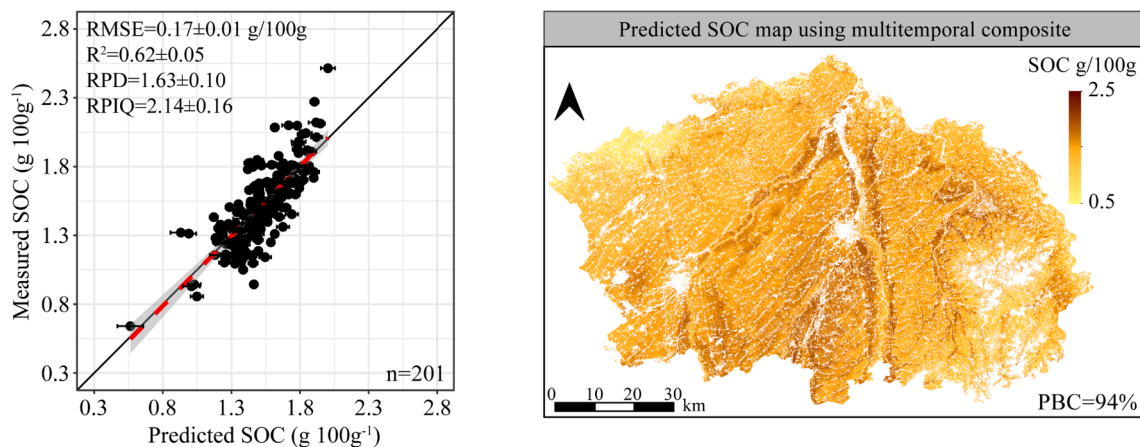


Fig. 6. Scatterplot of measured versus predicted soil organic carbon (SOC) for the Northeast China study region. 10-fold cross-validation was used to develop the PLSR model based on the multitemporal bare soil composite. The predicted SOC values are average values from 100 bootstrap model simulations, and the error bars represent standard deviations of the mean predicted SOC, as a measure of prediction uncertainty. The reported RMSE, R^2 , RPD and RPIQ values are also the mean values \pm the standard deviations of the 100 simulations. The black line is the 1:1 line while the red dashed line is the linear regression line. The developed PLSR model was applied to the entire bare soil composite to enable pixel-wise SOC predictions for a 10 m resolution map on the right, which is also the mean of 100 predicted maps. PBC denotes the percentage of bare soil coverage within the cropland extent. (For interpretation of the references to color in this figure legend, the reader is referred to the web version of this article.)

multitemporal bare soil composites, because only the high-quality images selected within optimal time-windows were included for creating the bare soil mosaic. Consequently, SOC prediction models developed from bare soil composites gave better (Table 2 and Fig. 6, NE China) or similar (Fig. 7, Belgian Loam belt) performances in comparison to those from single-date images. While maintaining a good prediction accuracy, the area of bare soil coverage for the Belgian study region increased roughly-two times from single-date to multitemporal analysis. A similar magnitude of increase was also reported by Diek et al. (2016) and Sil-vero et al. (2021), highlighting the major advantage of such multitemporal approaches to achieving spatially continuous SOC maps.

Compared to previous studies that used Sentinel-2 images to predict SOC, our model created with the multitemporal bare soil composites either had similar level of prediction accuracy or outperformed other studies, a majority of which were built with single-date images (Table 3). Specifically, RMSE varied substantially among different studies, due to the inherently distinct range of variations in SOC. This implies that comprehensive examination into model predictive performances should use more than one RMSE index. The highest R^2 was obtained in the NE China region of this study, followed by studies from Vaudour et al. (2019a) and Vaudour et al. (2021), who used both single-date and multitemporal approaches to predict SOC for the croplands in the Versailles Plain, France; this stresses once again the advantage of the multitemporal approach to maximize the mapped cropland area. For the Belgian study region, the multitemporal approach adopted in this study achieved similar RMSE and higher RPD than the single-date study by Castaldi et al. (2019b). Moreover, Shi et al. (2020a) used the Airborne Prism Experiment (APEX) hyperspectral imagery in the same Belgian Loam Belt region and achieved comparable model performance (R^2 : 0.52, RMSE: $0.19 \text{ g } 100 \text{ g}^{-1}$) to what was obtained in this study that used Sentinel-2 images with coarser spectral resolution.

The overall good model performance across the three study regions was also reflected in other aspects: (1) the SOC predictions were characterized by small uncertainties, suggesting the robustness of the developed prediction models; (2) investigations into the VIP scores of the PLSR models created with both resampled lab spectra and real Sentinel-2 data showed that similar bands were involved in controlling the SOC prediction. This implies that the physical relationship between spectral bands and SOC existing for laboratory spectra was also found in Sentinel-2 spectra. For both study regions, SOC was consistently found to be sensitive to variations in the NIR bands (B8 and/or B8A) and two

SWIR bands (B11 and B12), which are known to have relations to specific chemical bonds and organic compounds (Ben-Dor et al., 1997), corroborating again the validity to directly link soil chromophores with satellite-based soil reflectance.

5.2. Using temporally consistent Sentinel-2 images to create multitemporal composite

It is well established that the quality of the spectral images is crucial for quantitative assessment of soil properties (Ben-Dor et al., 2009). In this study, the designation of optimal time-windows is believed to be the main reason that secured images of high quality in terms of low cloud cover, maximal bare soil coverage and minimal spectral noise from external factors. Without making selective screening of Sentinel-2 images, Vaudour et al. (2019b) found that images acquired in different months produced drastically different SOC prediction performances, with R^2 ranging from 0.58 during the crop sowing period in spring characterized by optimal soil surface conditions to <0.1 for dates that were influenced by soil moisture and surface roughness, particularly during winter periods. In a more recent study, the same lead author adopted a “per-date” mosaicking approach that achieved good SOC prediction accuracy with larger bare soil coverage (Vaudour et al., 2021). They followed a similar philosophy as the optimal time-window pre-determination used in this study, together with exploration into the potential of Sentinel-1 data to account for soil moisture, in order to create a bare soil composite based only on single-date images that gave good individual performances.

Furthermore, we compared our approach against a non-selective approach that included all available cloudless images to create a bare soil composite, and found that, in NE China, almost identical model performances were obtained with or without setting an optimal time-window (Figs. 6 and 10), while in the Belgian Loam Belt, the model performance worsened if no optimal time-window was used for image screening (Figs. 7 and 10). This suggests that for NE China, the pre-determination of an optimal time-window was shown to be unnecessary for such monoculture systems, as bare soil typically only occur once per year during the annual sowing of maize. On the other hand, for regions where bare soil might occur at different times and during prolonged periods per year, the selection of optimal time-windows could help exclude bare soil pixels that are interfered by perturbing factors, such as crop residue, soil moisture, soil crusts, surface roughness, and

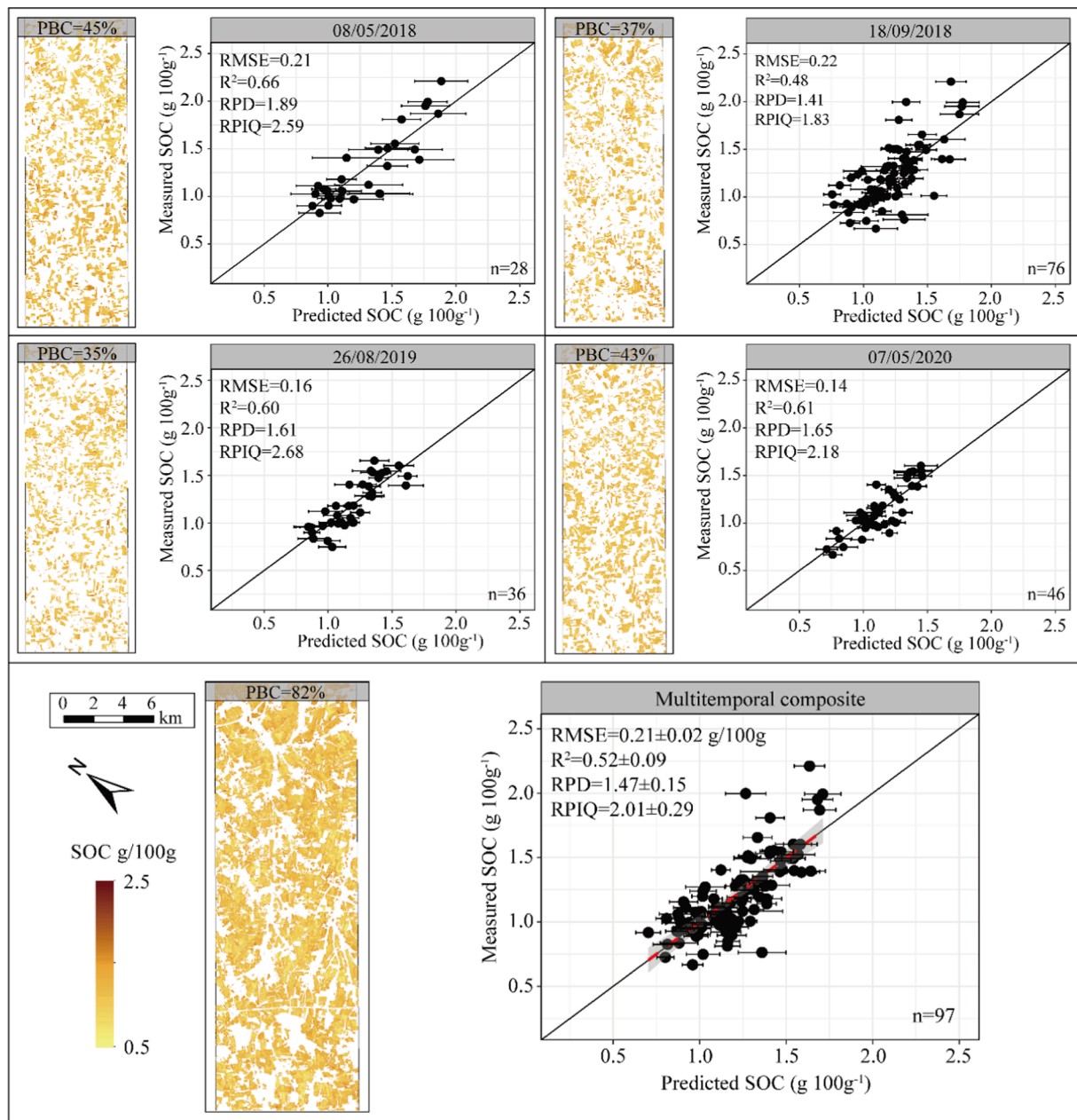


Fig. 7. Measured versus predicted soil organic carbon (SOC) for the Belgian Loam Belt study region based on the partial least squares regression (PLSR) models created using four single-date images as well as one multitemporal bare soil composite, and their corresponding SOC maps predicted with the PLSR models. 100 bootstrapped model simulations were conducted, and only mean results are presented together with their standard deviations. More details are given in Fig. 6. PBC is the percentage of bare soil coverage within the cropland extent.

reduced quality of atmospheric corrected images in winter months as sun elevation varies (Chabrilat et al., 2019; Vaudour et al., 2019b).

5.3. Spatial characterization of SOC dynamics with Sentinel-2 imagery

McBratney et al. (2003) developed the *scorpan*-type framework as the basis of classical digital soil mapping methods, the products of which often show compromised ability to capture localized soil heterogeneities, due to the general lack of up-to-date, high-resolution soil and environmental inputs (Vågen et al., 2016). Leveraging on recent advances in extracting bare soil spectra from Sentinel-2 composites, the goal of this study was to bring one step closer to achieving spatially continuous and real-time SOC mapping at high spatial resolution, thus allowing field-scale investigations into the spatial variability of SOC at two intensively cultivated regions.

Zoom-in SOC maps (Fig. 11) at selected areas revealed contrasting SOC patterns of the two study regions at fine scale, coinciding with the status of cropland management practices taken in these regions. In NE China, severe degradation processes (e.g., tillage and water erosion) at sloping croplands led to the exposure of light-colored subsoils, a commonly observed phenomenon in black soils (e.g., Chernozems, Phaeozems, Kastanozems) as indicated in the true color image (Fig. 11a) and reported elsewhere in the US Great Plain and Czech Republic (Thaler et al., 2021; Žizala et al., 2019). The fact that erosion-induced SOC redistribution pattern could be well-captured by Sentinel-2 based soil mapping has significant global implications, because, according to the FAO report (FAO, 2022), 30 % of global wheat production, 16 % of maize, and 46 % of barley come from black soils, a majority of which are facing degradation issues at present. In this line, the proposed approach could serve as an useful tool for high-resolution SOC and soil

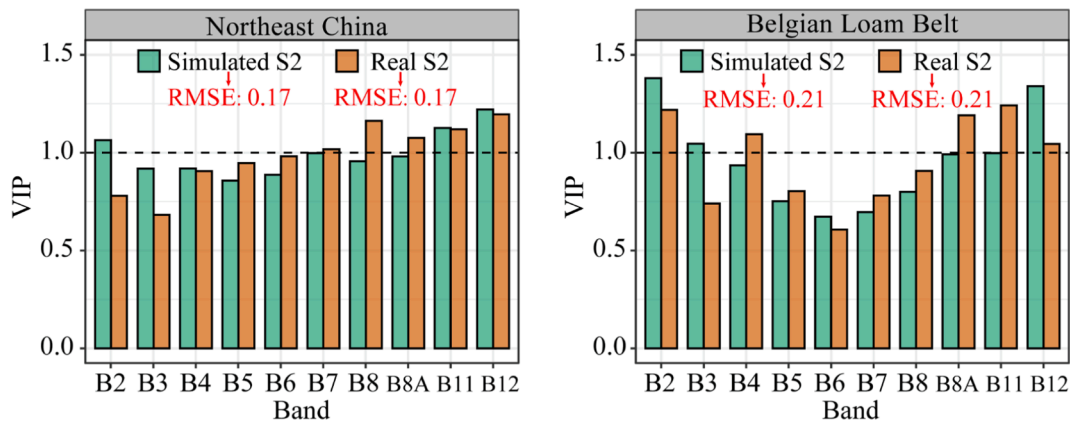


Fig. 8. Variable importance projection (VIP) in the partial least squares regression (PLSR) models using both simulated and real Sentinel-2 (S2) data. Spectral bands that have VIP scores larger than 1 are considered significant predictors in the PLSR models. Simulated S2 data were generated from the laboratory VNIR/SWIR (400–2500 nm) spectra, which were resampled into the same spectral resolution as the real S2. PLSR models developed with simulated and real S2 data achieved identical RMSE values for both study regions (see also Figs. 6 and 7).

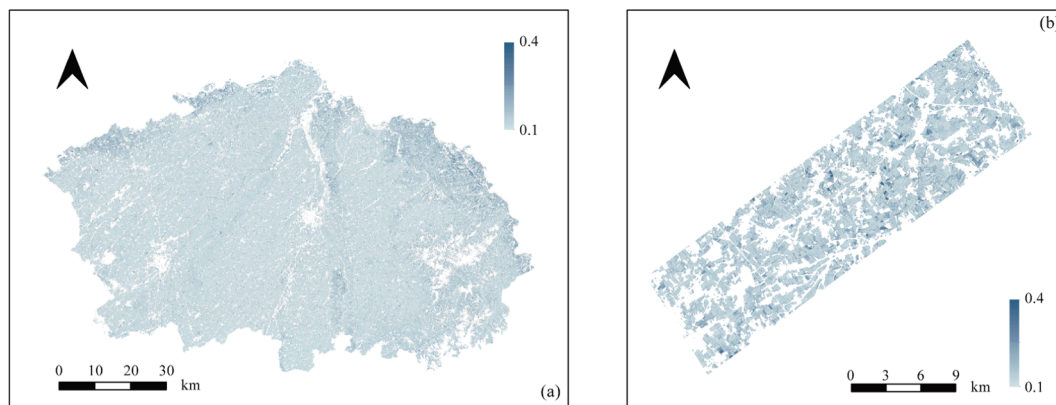


Fig. 9. Maps of uncertainties in SOC prediction for (a) NE China and (b) study regions expressed as the range of the 90 % prediction interval.

Table 3

Comparing the model performances in SOC prediction with previous studies that used Sentinel-2 imagery. RMSE: root mean squared error; R²: coefficient of determination; RPD: ratio of performance to deviation; RPIQ: ratio of performance to interquartile range. n.a. indicates that corresponding values were not reported by relevant studies.

| Study region | RMSE (g 100 g ⁻¹) | R ² | RPD | RPIQ | Approach | References |
|----------------------------|-------------------------------|----------------|------------|------------|---------------|--|
| Přestavlky, Czech Republic | 0.14 | n.a. | 1.6 | n.a. | Single-date | Gholizadeh et al. (2018) |
| Šardice, Czech Republic | 0.23 | n.a. | 1.7 | n.a. | | |
| Nová Ves, Czech Republic | 0.08 | n.a. | 1.7 | n.a. | | |
| Jičín, Czech Republic | 0.08 | n.a. | 1.9 | n.a. | | |
| Gutland-Oesling, Luxemburg | 0.30 | n.a. | 2.6 | n.a. | Single-date | Castaldi et al. (2019) |
| Demmin, Germany | 0.12 | n.a. | 2.2 | n.a. | | |
| Belgian Loam Belt | 0.19 | n.a. | 1.1 | n.a. | | |
| Versailles Plain, France | 0.12 | 0.56 | 1.5 | n.a. | Single-date | Vaudour et al. (2019) |
| Peyne Valley, France | 0.37 | 0.02 | 1.0 | n.a. | | |
| São Paulo, Brazil | 0.61 | 0.38 | n.a. | n.a. | Multitemporal | Silvero et al. (2021) |
| Versailles Plain, France | 0.33 | 0.54 | 1.5 | 2.2 | Multitemporal | Vaudour et al. (2021) |
| Northeast China | 0.17 | 0.62 | 1.6 | 2.1 | Multitemporal | This study |
| Belgian Loam Belt | 0.21 | 0.52 | 1.5 | 2.0 | | |

degradation assessment in the world’s black soil areas ([Gholizadeh et al., 2018](#)). In the Belgian Loam Belt, SOC variability showed a contrasting spatial pattern from NE China, as SOC distribution was more dictated by inter-field variability rather than intra-field, suggesting a dominant impact of field-specific management practices on SOC. The same finding was reported by [Zhou et al. \(2022\)](#), who found that the amount of organic inputs from varying crop rotations and cover cropping largely contributed to inter-field SOC variability in the croplands of Wallonia, Belgium. In summary, the multitemporal Sentinel-2 remote

sensing approach adopted in this study was shown capable of capturing field-scale SOC patterns at two regions with distinct degrees of soil degradation and cropland management.

From the SOC monitoring perspective, however, the ability of Sentinel-2 based SOC modelling approach adopted in this study to detect cropland SOC changes likely remains to be limited. For instance, [Yan et al. \(2011\)](#) reported a 15 % decrease in topsoil SOC content for the Chernozem region of NE China during a 30-year period (1980–2010). Taking the current average SOC content of 1.51 g 100 g⁻¹ ([Table 1](#)) in

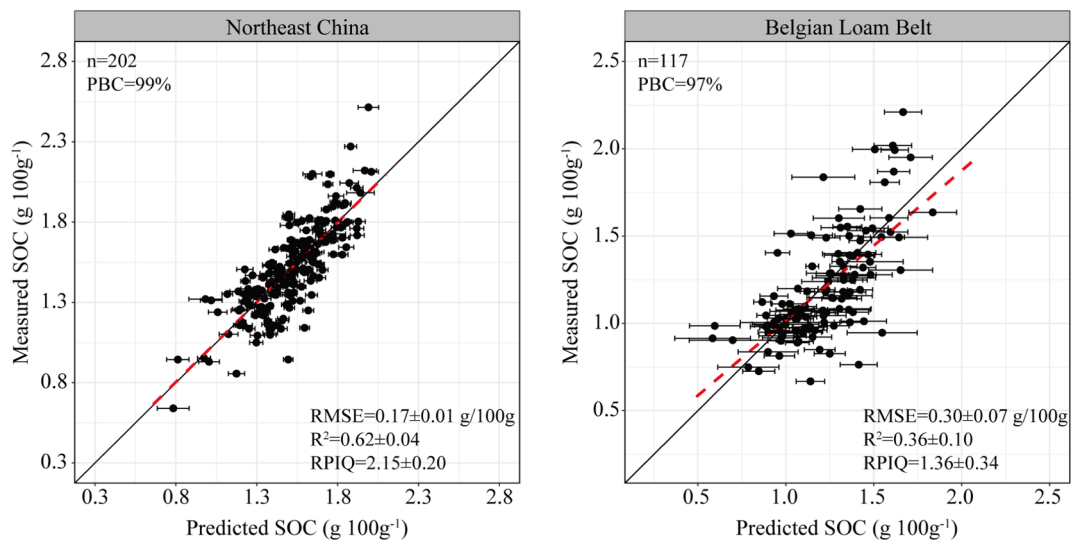


Fig. 10. Performances of soil organic carbon (SOC) prediction models based on a “non-selective” bare soil composite, encompassing all available cloudless Sentinel-2 images for the Northeast China and Belgian study regions. Total number of scenes used in creating the bare soil composites were 27 for Northeast China and 22 for the Belgian Loam Belt (see also Table 1). The bare pixel selection criteria, modelling approaches and presentation of results are the same with those from Figs. 6 and 7.

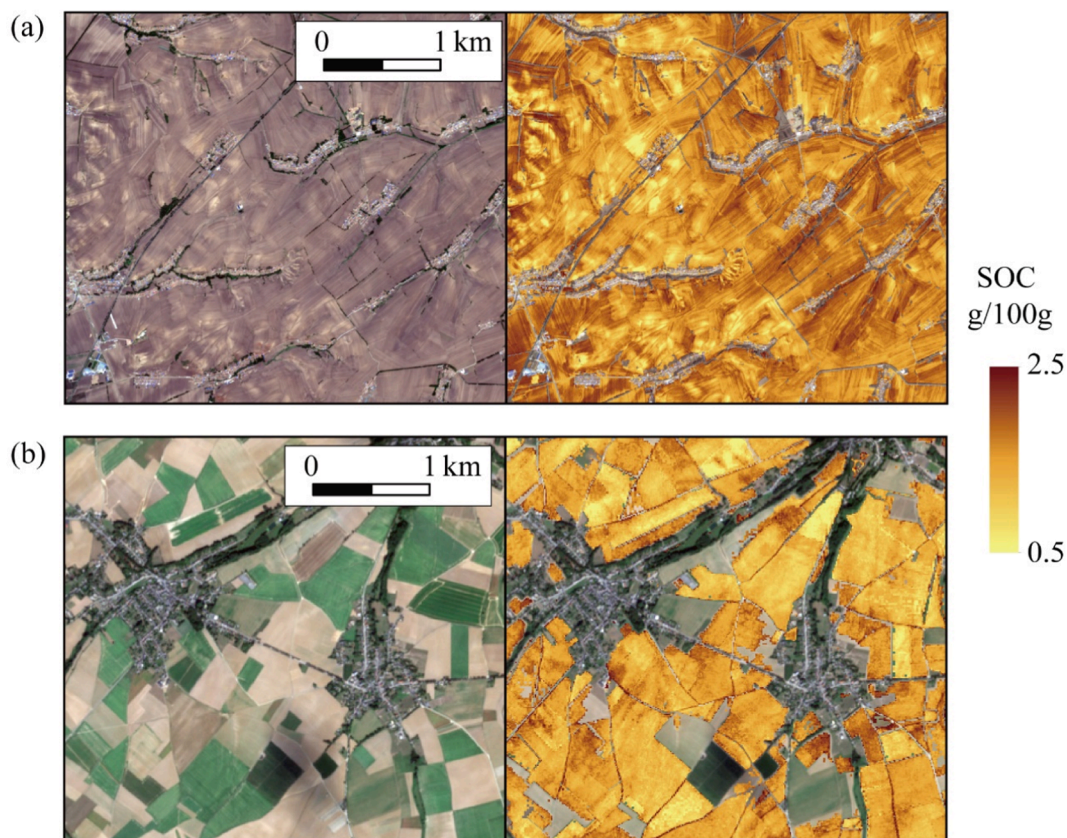


Fig. 11. Predicted soil organic carbon (SOC) map at selected areas for (a) Northeast China and (b) Belgium study regions. SOC map was overlaid onto Sentinel-2 true color images as shown on the left side of each row.

the study region as end reference, a 15 % decrease would correspond to a SOC change of $0.27 \text{ g } 100 \text{ g}^{-1}$, similar to the level of prediction uncertainty for the region with more than 90 % of pixels had prediction intervals (90 %) between 0.2 and $0.25 \text{ g } 100 \text{ g}^{-1}$ (Fig. 9). Repeated LUCAS surveys on European croplands in 2009 and 2015 revealed even smaller changes (2.49 % decrease) for the sampling points that remained as croplands during the 6-year period (Fernández-Ugalde et al., 2020).

5.4. Limitations and outlook

The spectra-based PLSR models yielded reasonable prediction accuracies, but there appeared to be consistent underestimation of high SOC values for both study regions (Figs. 5 and 7), possibly due to (1) the relatively small number of training samples in that range, and/or (2) the exclusive use of bare soil spectra without considering additional environmental covariates. For the former, more balanced sampling strategies in support of specific mapping objectives should be explored (Brus, 2019). For the latter, future studies should investigate to what extent combining vegetation, topographic, and pedoclimatic indices (Gholizadeh et al., 2018; Yang et al., 2020) with soil spectra can improve SOC prediction, but caution should be taken in the selection of covariates, given the controlling factors of SOC are likely to be scale-dependent (Lamichhane et al., 2019).

Admittedly, the use of bare soil spectra to map SOC also seemingly confronts against the promotion of SOC sequestration resulting from a diverse crop rotation, cover cropping, residue retention, and conservation tillage practices (Amelung et al., 2020), all of which would otherwise be regarded as disturbing factors if detection of bare soil pixels was desired. Rather than treating these as two paradoxical compartments, perhaps the way forward is to work the two in unison, where baseline soil information from bare soil spectra of different platforms (Tziolas et al., 2020) is linked with the account of field-specific management inputs (Zhou et al., 2022) to arrive at a more comprehensive framework of SOC mapping. Given that SOC prediction uncertainties associated with current spectral-based mapping approaches do not yet allow meaningful SOC monitoring at field scale, we speculate that perhaps only by explicitly incorporating cropland management data into the core of spectra-based SOC mapping, can we realistically expect to detect management-induced SOC changes from a remote sensing perspective. This will require a concerted effort to bridge future advances from various research fields in remote sensing and soil science.

Finally, Sentinel-2 based SOC mapping studies so far mostly focused on agricultural systems in temperate regions, while the largest SOC data gap lies in the global tropics dominated by small-holder agriculture. Future studies should therefore also be devoted to facilitating the further development and application of such methodology in tropical systems, where effective algorithms are needed to optimize the quality and quantity of bare soil pixels under frequent influence of cloud cover and mixed signals of soil and vegetation.

6. Conclusions

The capability of multitemporal Sentinel-2 remote sensing for spatially continuous SOC mapping in croplands was demonstrated in two contrasting agroecosystems of the NE China Chernozem region and the Belgian Loam Belt. A methodological framework, including delineation of cropland extent, detection of bare soil pixels with minimal disturbance, and creation of multitemporal bare soil composite, was established to achieve maximum cropland coverage in each study region. Optimal time-windows, corresponding to major crop sowing periods when soils are largely exposed and of minimal disturbance, were determined to ensure the inclusion of temporally stable and consistent single-date images for the generation of bare soil composites.

Spectral-based models developed from multitemporal composites consistently produced better or similar prediction accuracies than single-date images for the two study regions (R^2 : 0.52–0.62; RMSE:

0.17–0.21 $\text{g } 100 \text{ g}^{-1}$), while also achieved maximum cropland coverage (>82 %). Investigations into the significant spectral bands that contributed to the prediction of SOC suggested that the physical relationship between spectral bands and SOC existing for laboratory spectra was largely translated into Sentinel-2 platforms. This highlights the widespread applicability of multitemporal Sentinel-2 remote sensing for spatially continuous and high-resolution SOC mapping in regions with contrasting biophysical environments and agricultural systems.

Declaration of Competing Interest

The authors declare that they have no known competing financial interests or personal relationships that could have appeared to influence the work reported in this paper.

Acknowledgements

P. Shi is a postdoc fellow of the Fonds de la Recherche Scientifique—FNRS (Belgium). This study is partly funded by the National Natural Science Foundation of China via grant no. 41807059 and the Swiss National Science Foundation Postdoc.Mobility Fellowship. Comments and suggestions from the two anonymous reviewers significantly improved the manuscript.

References

- Amelung, W., Bossio, D., de Vries, W., Kögel-Knabner, I., Lehmann, J., Amundson, R., Bol, R., Collins, C., Lal, R., Leifeld, J., Minasny, B., Pan, G., Paustian, K., Rumpel, C., Sanderman, J., van Groenigen, J.W., Mooney, S., van Wesemael, B., Wander, M., Chabbi, A., 2020. Towards a global-scale soil climate mitigation strategy. *Nat. Commun.* 11, 5427.
- Angelopoulou, T., Tziolas, N., Balafoutis, A., Zalis, G., Bochtis, D., 2019. Remote sensing techniques for soil organic carbon estimation: A review. *Remote Sens.* 11, 676.
- Arrouays, D., Grundy, M.G., Hartemink, A.E., Hempel, J.W., Heuvelink, G.B.M., Hong, S. Y., Lagacherie, P., Lelyk, G., McBratney, A.B., McKenzie, N.J., Mendonca-Santos, M. d.L., Minasny, B., Montanarella, L., Odeh, I.O.A., Sanchez, P.A., Thompson, J.A., Zhang, G.-L., 2014. Chapter three - GlobalSoilMap: Toward a fine-resolution global grid of soil properties, in: Sparks, D.L. (Ed.), *Adv. Agron. Academic Press*, pp. 93–134.
- Ben-Dor, E., Inbar, Y., Chen, Y., 1997. The reflectance spectra of organic matter in the visible near-infrared and short wave infrared region (400–2500 nm) during a controlled decomposition process. *Remote Sens. Environ.* 61, 1–15.
- Ben-Dor, E., Chabrilat, S., Dematte, J.A.M., Taylor, G.R., Hill, J., Whiting, M.L., Sommer, S., 2009. Using Imaging Spectroscopy to study soil properties. *Remote Sens. Environ.* 113, S38–S55.
- Borrelli, P., Robinson, D.A., Panagos, P., Lugato, E., Yang, J.E., Alewell, C., Wuepper, D., Montanarella, L., Ballabio, C., 2020. Land use and climate change impacts on global soil erosion by water (2015–2070). *Proc. Natl. Acad. Sci.* 117, 21994–22001.
- Brus, D.J., 2019. Sampling for digital soil mapping: A tutorial supported by R scripts. *Geoderma* 338, 464–480.
- Castaldi, F., Chabrilat, S., Don, A., van Wesemael, B., 2019a. Soil organic carbon mapping using LUCAS topsoil database and Sentinel-2 data: An approach to reduce soil moisture and crop residue effects. *Remote Sens.* 11, 2121.
- Castaldi, F., Hueni, A., Chabrilat, S., Ward, K., Buttafuoco, G., Bomans, B., Vreys, K., Brell, M., van Wesemael, B., 2019b. Evaluating the capability of the Sentinel 2 data for soil organic carbon prediction in croplands. *ISPRS J. Photogramm. Remote Sens.* 147, 267–282.
- Chabrilat, S., Ben-Dor, E., Cierniewski, J., Gomez, C., Schmid, T., van Wesemael, B., 2019. *Imaging Spectroscopy for Soil Mapping and Monitoring. Surv. Geophys.* 40, 361–399.
- Chong, I.-G., Jun, C.-H., 2005. Performance of some variable selection methods when multicollinearity is present. *Chemomet. Intell. Lab. Syst.* 78, 103–112.
- Dematte, J.A.M., Fongaro, C.T., Rizzo, R., Safanelli, J.L., 2018. Geospatial Soil Sensing System (GEOS3): A powerful data mining procedure to retrieve soil spectral reflectance from satellite images. *Remote Sens. Environ.* 212, 161–175.
- Diek, S., Schaepman, M.E., De Jong, R., 2016. Creating multi-temporal composites of airborne imaging spectroscopy data in support of digital soil mapping. *Remote Sens.* 8, 906.
- Diek, S., Chabrilat, S., Nocita, M., Schaepman, M.E., de Jong, R., 2019. Minimizing soil moisture variations in multi-temporal airborne imaging spectrometer data for digital soil mapping. *Geoderma* 337, 607–621.
- Dvorakova, K., Shi, P., Limbourg, Q., van Wesemael, B., 2020. Soil Organic Carbon Mapping from Remote Sensing: The Effect of Crop Residues. *Remote Sens.* 12, 1913.
- FAO, 2022. *Global Map of Black Soils*, Rome, Italy.
- Fernández-Ugalde, O., Ballabio, C., Lugato, E., Scarpa, S., Jones, A., 2020. Assessment of changes in topsoil properties in LUCAS samples between 2009/2012 and 2015 surveys. *Publications Office of the European Union, Luxembourg*.

- Gholizadeh, A., Žizala, D., Saberioon, M., Borůvka, L., 2018. Soil organic carbon and texture retrieving and mapping using proximal, airborne and Sentinel-2 spectral imaging. *Remote Sens. Environ.* 218, 89–103.
- Gomez, C., Dharumarajan, S., Féret, J.-B., Lagacherie, P., Ruiz, L., Sekhar, M., 2019. Use of Sentinel-2 Time-Series Images for Classification and Uncertainty Analysis of Inherent Biophysical Property: Case of Soil Texture Mapping. *Remote Sens.* 11, 565.
- Helder, D., Markham, B., Morfitt, R., Storey, J., Barsi, J., Gascon, F., Clerc, S., LaFrance, B., Masek, J., Roy, D.P., Lewis, A., Pahlevan, N., 2018. Observations and Recommendations for the Calibration of Landsat 8 OLI and Sentinel 2 MSI for Improved Data Interoperability. *Remote Sens.* 10, 1340.
- Hengl, T., Mendes de Jesus, J., Heuvelink, G.B.M., Ruiperez Gonzalez, M., Kilibarda, M., Blagotić, A., Shangquan, W., Wright, M.N., Geng, X., Bauer-Marschallinger, B., Guevara, M.A., Vargas, R., MacMillan, R.A., Batjes, N.H., Leenaars, J.G.B., Ribeiro, E., Wheeler, I., Mantel, S., Kempen, B., 2017. SoilGrids250m: Global gridded soil information based on machine learning. *PLoS ONE* 12, e0169748.
- Lal, R., 2004. Soil carbon sequestration impacts on global climate change and food security. *Science* 304, 1623.
- Lamichhane, S., Kumar, L., Wilson, B., 2019. Digital soil mapping algorithms and covariates for soil organic carbon mapping and their implications: A review. *Geoderma* 352, 395–413.
- Lorenz, K., Lal, R., Ehlers, K., 2019. Soil organic carbon stock as an indicator for monitoring land and soil degradation in relation to United Nations' Sustainable Development Goals. *Land Degrad. Dev.* 30, 824–838.
- Malone, B.P., Minasny, B., McBratney, A.B., 2017. Some Methods for the Quantification of Prediction Uncertainties for Digital Soil Mapping. In: Malone, B.P., Minasny, B., McBratney, A.B. (Eds.), *Using R for Digital Soil Mapping*. Springer International Publishing, Cham, pp. 169–219.
- McBratney, A.B., Mendonça Santos, M.L., Minasny, B., 2003. On digital soil mapping. *Geoderma* 117, 3–52.
- Ou, Y., Rousseau, A.N., Wang, L., Yan, B., 2017. Spatio-temporal patterns of soil organic carbon and pH in relation to environmental factors—A case study of the Black Soil Region of Northeastern China. *Agric. Ecosyst. Environ.* 245, 22–31.
- Rizzo, R., Medeiros, L.G., Mello, D.C.d., Marques, K.P.P., Mendes, W.d.S., Quiñonez Silvero, N.E., Dotto, A.C., Bonfatti, B.R., Demattê, J.A.M., 2020. Multi-temporal bare surface image associated with transfer functions to support soil classification and mapping in southeastern Brazil. *Geoderma* 361, 114018.
- Rogge, D., Bauer, A., Zeidler, J., Mueller, A., Esch, T., Heiden, U., 2018. Building an exposed soil composite processor (SCMaP) for mapping spatial and temporal characteristics of soils with Landsat imagery (1984–2014). *Remote Sens. Environ.* 205, 1–17.
- Safanelli, J.L., Chabrilat, S., Ben-Dor, E., Demattê, J.A.M., 2020. Multispectral Models from Bare Soil Composites for Mapping Topsoil Properties over Europe. *Remote Sens.* 12, 1369.
- Sherrod, L., Dunn, G., Peterson, G., Kolberg, R., 2002. Inorganic carbon analysis by modified pressure-calculator method. *Soil Sci. Soc. Am. J.* 66, 299–305.
- Shi, P., Castaldi, F., van Wesemael, B., Van Oost, K., 2020a. Large-Scale, High-Resolution Mapping of Soil Aggregate Stability in Croplands Using APEX Hyperspectral Imagery. *Remote Sens.* 12, 666.
- Shi, P., Castaldi, F., van Wesemael, B., Van Oost, K., 2020b. Vis-NIR spectroscopic assessment of soil aggregate stability and aggregate size distribution in the Belgian Loam Belt. *Geoderma* 357, 113958.
- Silvero, N.E.Q., Demattê, J.A.M., Amorim, M.T.A., Santos, N.V.D., Rizzo, R., Safanelli, J. L., Poppiel, R.R., Mendes, W.D.S., Bonfatti, B.R., 2021. Soil variability and quantification based on Sentinel-2 and Landsat-8 bare soil images: A comparison. *Remote Sens. Environ.* 252.
- Soriano-Disla, J.M., Janik, L.J., Rossel, R.A.V., Macdonald, L.M., McLaughlin, M.J., 2014. The Performance of Visible, Near-, and Mid-Infrared Reflectance Spectroscopy for Prediction of Soil Physical, Chemical, and Biological Properties. *Appl. Spectrosc. Rev.* 49, 139–186.
- Thaler, E.A., Larsen, I.J., Yu, Q., 2021. The extent of soil loss across the US Corn Belt. *Proc. Natl. Acad. Sci.* 118 e1922375118.
- Tziolas, N., Tsakiridis, N., Ogen, Y., Kalopesa, E., Ben-Dor, E., Theocharis, J., Zalidis, G., 2020. An integrated methodology using open soil spectral libraries and Earth Observation data for soil organic carbon estimations in support of soil-related SDGs. *Remote Sens. Environ.* 111793.
- Vågen, T.-G., Winowiecki, L.A., Tondoh, J.E., Desta, L.T., Gumbricht, T., 2016. Mapping of soil properties and land degradation risk in Africa using MODIS reflectance. *Geoderma* 263, 216–225.
- Van Deventer, A., Ward, A., Gowda, P., Lyon, J., 1997. Using thematic mapper data to identify contrasting soil plains and tillage practices. *Photogramm. Eng. Rem. S.* 63, 87–93.
- Van Oost, K., Quine, T.A., Govers, G., De Gryze, S., Six, J., Harden, J.W., Ritchie, J.C., McCarty, G.W., Heckrath, G., Kosmas, C., Giraldez, J.V., da Silva, J.R.M., Merckx, R., 2007. The impact of agricultural soil erosion on the global carbon cycle. *Science* 318, 626–629.
- Vaudour, E., Gomez, C., Fouad, Y., Lagacherie, P., 2019a. Sentinel-2 image capacities to predict common topsoil properties of temperate and Mediterranean agroecosystems. *Remote Sens. Environ.* 223, 21–33.
- Vaudour, E., Gomez, C., Loiseau, T., Baghdadi, N., Loubet, B., Arrouays, D., Ali, L., Lagacherie, P., 2019b. The Impact of Acquisition Date on the Prediction Performance of Topsoil Organic Carbon from Sentinel-2 for Croplands. *Remote Sens.* 11, 2143.
- Vaudour, E., Gomez, C., Lagacherie, P., Loiseau, T., Baghdadi, N., Urbina-Salazar, D., Loubet, B., Arrouays, D., 2021. Temporal mosaicking approaches of Sentinel-2 images for extending topsoil organic carbon content mapping in croplands. *Int. J. Appl. Earth Obs. Geoinf.* 96, 102277.
- Yan, X., Cai, Z., Wang, S., Smith, P., 2011. Direct measurement of soil organic carbon content change in the croplands of China. *Glob. Change Biol.* 17, 1487–1496.
- Yang, H., Zhang, X., Xu, M., Shao, S., Wang, X., Liu, W., Wu, D., Ma, Y., Bao, Y., Zhang, X., Liu, H., 2020. Hyper-temporal remote sensing data in bare soil period and terrain attributes for digital soil mapping in the Black soil regions of China. *Catena* 184, 104259.
- Yue, Y., Ni, J., Ciaisi, P., Piao, S., Wang, T., Huang, M., Borthwick, A.G.L., Li, T., Wang, Y., Chappell, A., Oost, K.V., 2016. Lateral transport of soil carbon and land-atmosphere CO₂ flux induced by water erosion in China. *Proc. Natl. Acad. Sci.* 113, 6617–6622.
- Zhou, Y., Chartin, C., Van Oost, K., van Wesemael, B., 2022. High-resolution soil organic carbon mapping at the field scale in Southern Belgium (Wallonia). *Geoderma* 422, 115929.
- Žizala, D., Juricová, A., Zádorová, T., Zelenková, K., Minařík, R., 2019. Mapping soil degradation using remote sensing data and ancillary data: South-East Moravia, Czech Republic. *Eur. J. Remote Sens.* 52, 108–122.